Two-component Turing reaction-diffusion models can explain how mother centrioles break PLK4 symmetry to generate a single daughter

Zachary M. Wilmott[1,2], Alain Goriely[2] and Jordan W. Raff[1]

Affiliation:

[1]Sir William Dunn School of Pathology, University of Oxford, Oxford, OX1 3RE, United Kingdom

[2]Mathematical Institute, University of Oxford, Oxford, OX2 6GG, United Kingdom

Key Words:
PLK4, Centriole, Centrosome, Symmetry-breaking, reaction-diffusion system

Abstract

Centrioles are barrel-shaped structures that duplicate when a mother centriole gives birth to a single daughter that grows from its side. Polo-like-kinase 4 (PLK4), the master regulator of centriole biogenesis, is initially recruited around the mother centriole, but it rapidly breaks symmetry to concentrate at a single focus that defines the daughter centriole assembly site. Two previous studies used different molecular and mathematical models to simulate PLK4 symmetry breaking. Here, we extract the core biological principles from both models to formulate a new and conceptually-simple mathematical model in which phosphorylated and unphosphorylated species of PLK4 (either on their own, or in complexes with other centriole duplication proteins) form the two-components of a classic Turing reaction-diffusion system. These two components bind/unbind from the mother centriole at different rates, and so effectively diffuse around the mother at different rates. This allows a slow-diffusing "activator" species to accumulate at a single site on the mother, while a fast-diffusing "inhibitor" species rapidly diffuses around the rest of the centriole to suppress activator accumulation. We conclude that phosphorylated and unphosphorylated species of PLK4 can form a Turing reaction-diffusion system, allowing PLK4 to break symmetry and generate a single daughter centriole.

Introduction

Most human cells are born with a single pair of centrioles comprising an older 'mother' and a younger 'daughter'; these organelles play an important part in many aspects of cellular organisation (Nigg and Raff, 2009; Bettencourt-Dias et al., 2011; Bornens, 2021; LeGuennec et al., 2021). This centriole pair must duplicate precisely once during each cell division cycle to ensure that a single centriole pair is passed on to each new daughter cell (Figure 1A) (Fırat-Karalar and Stearns, 2014; Nigg and Holland, 2018; Banterle and Gönczy, 2017). The centriole is a 9-fold symmetric structure and it is unclear how this symmetry is broken to establish a single centriole assembly site. Polo-like-kinase 4 (PLK4) is the master regulator of centriole biogenesis and it helps define the site of daughter centriole assembly: new centrioles cannot assemble in the absence of PLK4 activity (Habedanck et al., 2005; Bettencourt-Dias et al., 2005; Wong et al., 2015), and mother centrioles produce too many daughters when PLK4 levels are increased (Kleylein-Sohn et al., 2007; Peel et al., 2007; Rodrigues-Martins et al., 2007; Basto et al., 2008; Rogers et al., 2009; Cunha-Ferreira et al., 2009; Holland et al., 2010; Guderian et al., 2010). PLK4 appears to be initially recruited around the entire surface of the mother centriole before, in a poorly understood process, it becomes concentrated at a single focus that defines the daughter centriole assembly site (Figure 1B) (Arquint and Nigg, 2016; Nigg and Holland, 2018; Gönczy and Hatzopoulos, 2019; Yamamoto and Kitagawa, 2021).

Two different mathematical models have recently been proposed to explain how PLK4 asymmetry might be generated. In the first approach, developed by Goryachev and colleagues (Leda et al., 2018), the centriolar surface is modelled as a number of discrete compartments that bind cytoplasmic PLK4 and the key centriole-assembly protein STIL. These two proteins interact both in the cytoplasm and on the centriole surface, with exchange

between the centriole compartments occurring via the shared cytoplasm. Crucially, the phosphorylation of STIL by PLK4 is postulated to increase the centriolar retention of the phosphorylated PLK4:STIL complexes. Since PLK4 can promote its own activation (Lopes et al., 2015; Moyer et al., 2015; Klebba et al., 2015), this system forms a positive feedback loop in which PLK4 activity locally auto-amplifies itself by phosphorylating PLK4:STIL complexes to strengthen their centriolar retention. This process creates a competition between the different compartments for binding to the various PLK4:STIL complexes. These chemical reactions were formulated as a system of ordinary differential equations (ODEs), and this system breaks symmetry robustly to establish a single dominant compartment that concentrates the phosphorylated PLK4:STIL complexes.

The second approach, developed by Kitagawa and colleagues (Takao et al., 2019), was motivated by the observations that PLK4 has an intrinsic ability to self-organise into macromolecular condensates in vitro (Montenegro Gouveia et al., 2018; Yamamoto and Kitagawa, 2019; Park et al., 2019), and that PLK4 and its centriole receptor CEP152 initially appear to be organised into discrete compartments around the centriole—~12 for CEP152 and ~6 for PLK4 (Takao et al., 2019). The authors assume that PLK4 initially binds equally well to the twelve CEP152 compartments and that, due to its self-assembling properties, this PLK4 then recruits additional PLK4. They allow PLK4 to autoactivate itself as the local concentration of PLK4 rises, and suppose that active PLK4 is more mobile in the condensates than inactive PLK4 (as observed experimentally). Thus, the active PLK4 generated in one compartment can diffuse to nearby compartments, activating their PLK4, which stimulates the PLK4 to leave the nearby compartment. In this way, each of the 12 CEP152 compartments effectively compete to recruit PLK4, which can then diffuse away and “laterally inhibit” recruitment at nearby

compartments. This process allows the 12 CEP152 compartments to generate a “pre-pattern” of 6 PLK4 compartments. At the start of S-phase, the addition of STIL and/or Sas-6 into the system generates additional positive feedback and ensures that the pre-patterned site with most PLK4 becomes the single dominant site.

From a mathematical perspective, each of these approaches has benefits and drawbacks. The advantage of the first approach is that the general setting allows the complex relationships between the components to be modelled in full. It enables the authors to examine the dominant reaction pathways that emerge from the complex dynamics (Leda et al., 2018). However, the underlying mathematical features of the model that enable symmetry breaking are potentially obscured by the complexity of the model (which comprises ~28 reaction parameters). In contrast, by allowing the components to transfer between compartments directly, the second model has significantly fewer parameters (Takao et al., 2019). However, the coarseness of the discretisation limits the number of patterns that the solution may form, and the robustness of the solution (i.e. the initial 6-fold PLK4 symmetry) is highly dependent on the initial discretisation (i.e. the 12-fold symmetry of the CEP152 compartments).

From a biology perspective, both models rely on assumptions and/or make predictions that are perhaps not fully consistent with current data. In the Takao et al. model, for example, the 12-fold symmetry of the CEP152 Receptor and 6-fold symmetry of the PLK4 pre-pattern have not been robustly observed in other systems (Tian et al., 2021; Wainman, 2021; Gao et al., 2021; Wilmerding et al., 2023). In the Leda et al. model, PLK4 phosphorylates PLK4:STIL complexes to promote their centriole-retention, predicting that inhibiting PLK4 kinase activity would reduce the retention of PLK4 at centrioles. But, inhibiting PLK4 activity seems to lead

to PLK4's accumulation at the centriole (Ohta et al., 2018; Yamamoto and Kitagawa, 2019). Moreover, the different mathematical frameworks used make it difficult to compare the two models, and also to assess whether other reaction regimes might be capable of generating PLK4 symmetry breaking.

Here, we propose the alternative approach of modelling PLK4 symmetry breaking as a "Turing system"; which we define here as a two-component reaction-diffusion system that breaks symmetry through activator-inhibitor dynamics. Such systems fall into one of two classes in which symmetry is broken through "long-range activation, short range inhibition" (Turing, 1952; Gierer and Meinhardt, 1972). Turing systems are famous for their ability to produce complex spatial patterns, and have been studied in relation to numerous phenomena including the formation of animal coats, predator-prey dynamics, and the spread of disease (Bard, 1981; Levin and Segel, 1985; Mimura and Murray, 1978; Sun, 2012). Although the two existing mathematical models of PLK4 symmetry breaking appear to be very different, we show that both may be redeveloped as two-component Turing systems, allowing the reaction schemes contained within them to be compared and analysed within a simple unifying framework. We demonstrate that models formulated using this framework can robustly break the initial symmetry of PLK4 around the centriole surface to form a single PLK4 peak. Moreover, overexpressing PLK4 in such models can lead to the formation of multiple PLK4 peaks, while inhibiting PLK4 kinase activity can lead to a loss of symmetry breaking and the uniform accumulation of PLK4 around the centriole surface—as observed experimentally. Perhaps surprisingly, when the two previous models are reformulated as such Turing systems, it becomes apparent that, in the appropriate parameter regime, the dominant chemical reactions that drive symmetry breaking in the two systems are actually the same.

In summary, we conclude that Turing reaction-diffusion systems provide an excellent framework for studying PLK4 symmetry breaking, and that the organisation of PLK4 into such a two-component system (with phosphorylated/unphosphorylated species of PLK4 potentially forming the two components) could explain how centrioles robustly define a single assembly site for their new daughters. Our hope is that the formalisation presented in this paper will simplify future investigation into PLK4 symmetry breaking, since the reaction-diffusion framework readily permits the study and comparison of numerous reaction schemes.

Results

Throughout this paper, we model the recruitment of PLK4 around the surface of the centriole as a two-component reaction-diffusion system acting on a one-dimensional ring (the centriole surface). It may be shown mathematically that the probabilistic random walk of a molecule that repeatedly binds to, and then unbinds from, a surface on the microscale acts as a diffusive process on the macroscale (Skellam, 1973). Therefore, we use surface diffusion as a simplifying modelling approximation for diffusion through the bulk, where the effective diffusion rate of a molecule along the surface (in our case the centriole surface) is directly related to the rate at which the molecule binds-to/unbinds-from that surface. The two components in such systems are always a slowly diffusing (i.e. rapidly binding and/or slowly unbinding) species termed an Activator (A), and a rapidly diffusing (i.e. slowly binding and/or rapidly unbinding) species termed an Inhibitor (I), which satisfy

$$\frac{\partial A}{\partial t} = f(A, I) + D_A \frac{\partial^2 A}{\partial x^2} \tag{1}$$

$$\frac{\partial I}{\partial t} = g(A, I) + D_I \frac{\partial^2 I}{\partial x^2} \tag{2}$$

where t is time, x is arc length (i.e. position) along the circular centriole surface, f and g are prescribed functions that describe the chemical reactions that determine how A and I accumulate and decay over time around the centriole surface, and D_A and D_I are the diffusivities of A and I on the centriole surface, respectively. We use this model as our basic framework.

In order for such a general reaction-diffusion system to break symmetry (i.e. to be a Turing system), there are two conditions that the model must satisfy (Ruan, 1998). First, there must

exist a steady state (independent of x and t) that is stable in the absence of diffusion. Second, this steady state must be unstable in the presence of diffusion. Such a system can break symmetry if the relatively fast chemical reactions initially drive the system towards the steady state, but this becomes destabilised by diffusion, which drives the pattern-forming instability over a longer time-scale. These conditions put constraints on the values of the parameters appearing in the equations that can support symmetry breaking. Mathematically, these constraints can be expressed, for any given system, as a set of inequalities that define the possible range of parameter values that will support symmetry breaking. As a consequence of these constraints, symmetry breaking requires that the activator and inhibitor in these systems only interact with each other in one of two well-defined regimes (Type I and Type II, Figure 1C). Crucially, in both regimes, the inhibitor must diffuse more rapidly than the activator in order to drive a process known as 'short-range activation, long-range inhibition'. An in-depth derivation and analysis of the stability criteria for such activator-inhibitor systems can be found in (Ruan, 1998), and we summarise the key results in Appendix I.

Model 1: Activator Conversion (based on the model of Takeo et al., 2018).

The first model we analyse is the "Activator Conversion" case in which a slowly-diffusing activator A (PLK4) is converted into a rapidly-diffusing inhibitor I (PLK4*) via phosphorylation (Figure 2A). As an example of such a model, we adapt the model originally proposed by Takeo et al., in which unphosphorylated (and so kinase inactive) PLK4 is initially recruited to the centriole surface where is starts to self-assemble into slowly turning-over macromolecular condensates. As PLK4 levels in the condensates increase, Takeo et al. allow PLK4 to auto-phosphorylate itself creating PLK4*, which turns-over more rapidly within the condensates, as observed *in vitro* (Montenegro Gouveia et al., 2018; Yamamoto and Kitagawa, 2019; Park

et al., 2019). Thus, in our reformulation of this model as a Turing system (Figure 2A), PLK4 functions as an activator because it recruits more PLK4 into the system, and it is slow diffusing because it turns over relatively slowly within the centriolar condensates. In contrast, PLK4* functions as an inhibitor because it suppresses the amount of activator (PLK4) in the system (by converting PLK4 to PLK4*), and it is rapidly-diffusing because it turns-over more rapidly within the centriolar condensates.

Takao et al. assume that the non-phosphorylated PLK4 self-assembly rate is subject to a sigmoidal attenuation (i.e. as the condensates grow, they become less likely to disassemble) because the central regions of the condensate become progressively more isolated from the cytoplasm as the condensate grows. We also adopt this sigmoidal self-assembly relationship in our model. However, whereas Takeo et al. assume that PLK4 (A) and PLK4* (I) are restricted to binding to a defined number of discrete, spatially-organised compartments around the periphery of the centriole, in our model we allow both species to bind freely anywhere on the centriole surface. This model reads

$$\frac{\partial A}{\partial t} = \boxed{\frac{aA^2}{1+A}} - \boxed{bA\sqrt{I}} - \boxed{cA} + \boxed{D_A \frac{\partial^2 A}{\partial x^2}} \tag{3}$$

$$\frac{\partial I}{\partial t} = \boxed{bA\sqrt{I}} - \boxed{dI} + \boxed{D_I \frac{\partial^2 I}{\partial x^2}} \tag{4}$$

The boxed parts of the equation describe how A (eq. 3) or I (eq. 4) are produced (*red*), removed (*blue*) or diffuse (*magenta*) within the system. The rate parameters a, b, c, and d correspond to the self-assembly rate of the unphosphorylated PLK4 complex (a), the phosphorylation rate of PLK4 by phosphorylated PLK4* (b), and the degradation/loss rate of unphosphorylated PLK4 (c) and phosphorylated PLK4* (d). The precise functional form of these equations, which correspond to the strength of the self-assembly of PLK4 and the

strength of trans-autophosphorylation of inactive PLK4 by active PLK4*, respectively, are discussed in Appendix II, where we also derive the symmetry-breaking criteria for this system. The conditions for symmetry breaking take the form of a set of inequalities for the parameters a, b, c, and d. Below, we choose simple parameter values $a = d = 200$, $b = 100$, $c = 0$, that satisfy these conditions (we evaluate the robustness of symmetry breaking to changes in these parameters later).

In Figure 2B, we plot the solution of this model (i.e. a computer simulation of how PLK4 (A) and PLK4* (I) levels vary over time along the centriole surface, from 0 to 2π) in the case that $D_A = 5$, and $D_I = 1000$ subject to the initial conditions $A = A_0(1 + W_A(x))$ and $I = I_0(1 + W_I(x))$. Here, A_0 and I_0 are the homogeneous steady-state solutions to (3) and (4), and W_A and W_I are independent random variables with uniform distribution on $[0, 1]$ that we use to generate the initial stochastic noise in the binding of A and I to the centriole surface at $t = 0$. We observe that this initial noise is rapidly suppressed as the system approaches a near-steady state where the amount of A and I recruited to the centriole surface are nearly constant around the entire centriole surface (Figure 2B, $t = 0$ to $t = 0.1$). However, on longer time-scales, this would-be steady-state is destabilised by the presence of diffusion in the system (Figure 2B, $t = 0.2$). This is due to the fact that any region in which the levels of A are slightly raised are reinforced due to the self-promotion of A. The same effect also increases I, but, since I rapidly diffuses away, the local accumulation of A is maintained while the production of A is inhibited around the rest of the centriole surface due to the excess I. The solution therefore robustly resolves to a non-homogeneous steady state with a single dominant peak (Figure 2B, $t = 1$). We note that, as instabilities are first developing after the

initial smoothing period, the solution displays two small peaks at approximately π separation before resolving to a single dominant peak.

As described in the Introduction, it has been shown experimentally that overexpressing PLK4 leads to the generation of multiple PLK4 foci around the mother centriole, whereas inhibiting PLK4 kinase activity prevents PLK4 symmetry breaking and PLK4 instead becomes evenly distributed at high levels around the centriole surface. To test if Model 1 could recapitulate these behaviours, we first simulated PLK4 overexpression by doubling the rate parameter a, the rate of PLK4 accumulation at the centriole, which is proportional to the cytoplasmic concentration of PLK4. This led to an increase in the number of stable steady-state centriolar peaks of both A (non-phosphorylated PLK4) and I (phosphorylated PLK4) species (Figure 2C). We then simulated the effect of PLK4 kinase inhibition by halving the phosphorylation rate parameter, b. We observed that PLK4 symmetry was no longer broken, and that PLK4 accumulated evenly around the centriole to a high steady-state level (Figure 2D). This happens because less I (PLK4*) is produced when PLK4 kinase activity is reduced, so I can no longer suppress the accumulation of A (inactive PLK4) around the centriole. We conclude that Model 1 can capture well three key features of PLK4 behaviour at the centriole: (1) Breaking symmetry to a single peak under normal conditions; (2) Breaking symmetry to multiple peaks when PLK4 is overexpressed; (3) Failing to break symmetry when PLK4 kinase activity is inhibited.

To test the robustness of PLK4 symmetry breaking in this model we created a phase-diagram by varying both the cytoplasmic concentration of Plk4 (a) and the kinase activity of PLK4 (b) (Figure 3A). Each point in the diagram shows the average number of PLK4 peaks observed at

a particular value of a and b averaged over 20 simulations. We observe a reasonably large region where PLK4 robustly breaks symmetry to produce a single peak (*teal* colour), indicating that the model is reasonably robust to changes in a and b. As expected, however, increasing the concentration of Plk4 in the cytoplasm, a, can lead to multiple PLK4 peaks being produced (*yellow* region), while the model is unable to break symmetry if the concentration or activity of PLK4 is too low (*dark blue* region). We also built a phase-diagram to study the effect of varying activator diffusivity (D_A) and inhibitor diffusivity (D_I) (Figure 3B). We see that the ratio of the diffusivities of the inhibitor to activator needs to be sufficiently large in order for the system to exhibit the short-range activation and long-range inhibition that is required for symmetry breaking. We also see that decreasing the diffusivities of both species (while maintaining an appropriate ratio) leads to a progressively increasing number of observed peaks. This is because, as the diffusivity decreases, information travels more slowly around the centriole surface and therefore distinct regions are able to break symmetry and produce peaks independently of each other.

Model 2: Inhibitor Conversion (based on the model of Leda et al., 2018).

The second model we examine is the "Inhibitor Conversion" case in which a rapidly-diffusing inhibitor (I) is converted into a slowly-diffusing activator (A) through phosphorylation (Figure 4A). As we describe below, the PLK4 symmetry breaking model proposed by Leda et al. may be reinterpreted as such a model, so we adapt the reaction regime proposed by these authors for this model.

The original Leda et al. system comprises just two proteins, PLK4 and STIL, but these combine to create four components defined by the phosphorylation state of each component, $[PS]$,

$[P^*S]$, $[PS^*]$, and $[P^*S^*]$ (* denoting phosphorylation). The authors assume that each component may be converted into another, both in the cytoplasm and at the centriole surface, through phosphorylation/dephosphorylation, and that the $[P^*S^*]$ species promotes the phosphorylation of all the other species. Crucially, the centriole complexes in which STIL is phosphorylated are postulated to exchange with the cytoplasm at a significantly slower rate than the complexes in which STIL is not phosphorylated (this will be the basis for the difference in the diffusion rates of the two-component system we formulate below). As in the Takeo et al. model, Leda et al. allow the complexes to bind to discrete centriole compartments, but there is no ordering or spatial orientation of these compartments. Instead, compartmental exchange occurs through the shared cytoplasm.

By reinterpreting this cytoplasmic exchange as a diffusive process—with diffusivity dependent on the rate of exchange—we develop a Turing system based on the reactions of the Leda et al. model. In our model, the two relevant components in the system are not PLK4 and STIL, but rather PLK4:STIL complexes that act as either fast-diffusing Inhibitors (I) (comprising PLK4 bound to non-phosphorylated STIL—$[PS]$ and $[P^*S]$) or slow-diffusing Activators (A) (comprising PLK4 bound to phosphorylated STIL, which exchange more slowly than the PLK4 complexes bound to non-phosphorylated STIL—$[PS^*]$ and $[P^*S^*]$). As in the original Leda et al. model, we allow the rapidly-diffusing I to be converted into the slowly-diffusing A by the phosphorylation of STIL (Figure 4A). The derivation of this model is given in detail in Appendix III which leads to the system:

$$\frac{\partial A}{\partial t} = \boxed{bIA^2} - \boxed{cA} + \boxed{D_A \frac{\partial^2 A}{\partial x^2}} \tag{5}$$

$$\frac{\partial I}{\partial t} = \boxed{a} - \boxed{bIA^2 - dI} + \boxed{D_I \frac{\partial^2 I}{\partial x^2}} \tag{6}$$

As before, the boxed parts of the equation describe how A (eq. 5) or I (eq. 6) are produced (*red*), removed (*blue*) or diffuse (*magenta*) within the system. Here, a is a constant source term for I (i.e. the rate at which phosphorylated and non-phosphorylated PLK4 form complexes with STIL), b is the rate at which I is converted into A, (i.e. the rate at which STIL is phosphorylated within these complexes), and c and d are the rates at which A and I degrade/dissociate, respectively. The conditions that the parameters a, b, c, and d must satisfy for the solutions to exhibit symmetry-breaking is given in Appendix III. Below, we choose simple parameter values $a = d = 200$, $b = 100$, $c = 0$, that satisfy these conditions.

In Figure 4B, we plot the solution output in the case that $D_A = 5$, and $D_I = 5000$ subject to the initial conditions $A = A_0(1 + W_A(x))$ and $I = A_I(1 + W_I(x))$, where A_0 and I_0 are the homogeneous steady-state solutions to (5) and (6) and W_A and W_I are independent random variables with uniform distribution on $[0, 1]$. As with Model 1, the solution approaches a stable non-homogeneous steady state with a dominant peak after an initial smoothing period. In contrast to model 1, we observe that in the region of the activator peak the inhibitor exhibits a slight dip. This is because, in Model 1, the activator promotes the production of the inhibitor, whereas in Model 2 the activator suppresses the production of the inhibitor (by promoting its conversion to the activator). In Figure 4C, we show the response of Model 2 to the overexpression of PLK4 by plotting the solution output when a (the rate of production of non-phosphorylated PLK4:STIL complexes) is doubled. As with Model 1, we find that this results in the formation of multiple peaks of A (PLK4 bound to phosphorylated STIL). In Figure 4D, we model the effect of inhibiting PLK4 kinase activity by halving the phosphorylation rate parameter, b. As with Model 1, we find that symmetry is no longer broken and that I

accumulates uniformly around the centriole. In contrast to Model 1, however, A (PLK4 bound to phosphorylated STIL) vanishes entirely from the centriole surface.

These conclusions may also be drawn from the phase-diagram showing the number of PLK4 peaks formed in the system as the cytoplasmic concentration of PLK4:STIL (a) and its kinase activity (b) are varied (Figure 3C). As with Model 1, there is a reasonably large region in the parameter space that corresponds to a single peak (teal colour), indicating the robustness of the model. In contrast to Model 1, however, we see that although increasing the cytoplasmic concentration of PLK4 initially leads to multiple PLK4 peaks, a critical value is eventually reached at which symmetry is no longer broken. We also give the phase-diagram for the number of peaks observed as D_A and D_I are varied, observing qualitatively similar results to the Model 1 case (Figure 3D).

Unifying the models of Takeo et al., and Leda et al.

At a first glance, the original models of Takao et al. and Leda et al. appear to be very different: they use different mathematical methods to describe different chemical reactions, with symmetry breaking in the former being driven by PLK4 phosphorylation and in the latter by the phosphorylation of STIL in complexes with PLK4. In deriving Model 2, we grouped together the species $A = [PS^*] + [P^*S^*]$ and $I = [PS] + [P^*S]$ based on the unbinding rates of the four species specified in the Leda et al. paper—where complexes containing phosphorylated STIL ($[PS^*]$ and $[P^*S^*]$) unbind slowly and those containing non-phosphorylated STIL ($[PS]$ and $[P^*S]$) unbind rapidly. It is simple, however, to modify these model parameters so that the unbinding rate now depends on the phosphorylation state of PLK4 in these complexes (as is the case in the Takeo et al. model), rather than on the phosphorylation state of STIL—i.e. if

we allow $[P^*S]$ and $[P^*S^*]$ to now unbind rapidly and $[PS]$ and $[PS^*]$ to now unbind slowly (by simply exchanging the values of rate parameters k_{11} and k_{12} in the Leda et al. paper). In this scenario, if we set $A = [PS] + [PS^*]$ and $I = [P^*S] + [P^*S^*]$ then, following the same procedure as before (see Appendix III), we arrive at a new model,

$$\frac{\partial A}{\partial t} = a - bAI^{\alpha} - cA + D_A \frac{\partial^2 A}{\partial x^2} \tag{7}$$

$$\frac{\partial I}{\partial t} = bAI^{\alpha} - dI + D_I \frac{\partial^2 I}{\partial x^2} \tag{8}$$

We observe that by setting $\alpha = 1/2$ and substituting the sigmoidal self-assembly source term $aA^2/(1 + A)$ in place of the constant source term, a, we obtain *exactly* Model 1. In other words, all of the dynamics of the Takao et al. model is contained within the Leda et al. model, but with additional complexity and a different choice of rate parameters.

Modelling symmetry breaking on a compartmentalised centriole surface

In our modelling so far, PLK4 symmetry breaking occurs on a continuous centriole surface; it does not require that the centriole surface be divided into discrete compartments that effectively compete with each other to become the dominant site (as is assumed in the previous models). Importantly, however, our model still applies if we divide the centriole surface into an arbitrary number of discrete compartments, with the various PLK4 species diffusing between these compartments laterally. In Figure 5, we show the system outputs of Model 1 (Figure 5A) and Model 2 (Figure 5B) when we run simulations with a centriole surface comprising 9 discrete compartments that interact with the various PLK4 species. In both instances, the systems robustly break their initial symmetry to produce a single dominant compartment that accumulates the relevant species.

Discussion

PLK4 is the master regulator of centriole biogenesis, so understanding how it becomes concentrated at a single site on the side of the mother centriole is crucial to understanding how centriole numbers are so strictly controlled (Fırat-Karalar and Stearns, 2014; Loncarek and Bettencourt-Dias, 2018; Nigg and Holland, 2018; Breslow and Holland, 2019). Two mathematical models have been previously proposed to explain PLK4 symmetry breaking, but they use distinct mathematical frameworks and invoke what appear to be very different reaction regimes (Leda et al., 2018; Takao et al., 2019). How can one compare these models? And how many other potential reaction regimes might be capable of generating PLK4 symmetry breaking?

To help address these questions, we have developed the alternate approach of modelling PLK4 symmetry breaking as a simple two-component "Turing system". Mathematically, such models can be classified as either "activator-inhibitor" (Type I) or "depletion" (Type II) systems depending on their reaction dynamics (Gierer and Meinhardt, 1972; Ruan, 1998) (Figure 1C). Type I systems require that the activator (A) promotes and the inhibitor (I) inhibits the production of both species, whereas Type II systems require that A inhibits the production of I, and that I promotes the production of A (Figure 1C). Crucially, both classes require that I diffuses faster than A. This is so that any local increase in A will reinforce itself, whereas any local increase in I is smoothed due to its rapid diffusion. This allows for A to accumulate initially at a particular site which then acts as either a global source (Type I) or sink (Type II) of I. This global source/sink of I regulates the amount of each species elsewhere in the domain—in particular suppressing the accumulation of A around the rest of the system.

We used this relatively simple and well-studied mathematical framework to present two models for PLK4 symmetry breaking; we first presented a Type I model based on the reaction schemed proposed by Takeo et al.; we then presented a Type II model, based on the reaction scheme proposed by Leda et al. Importantly, although the previous models proposed different reaction regimes and used different mathematical methods, we conclude that the symmetry-breaking properties of both models may ultimately be described by Turing system dynamics. In the case of the Leda et al. model, this means that the dominant reaction pathways that lead to symmetry breaking can be retained while reducing the model from 11 components to 2. Furthermore, we showed that if this model is modified in such a way that the retention rate of the PLK4:STIL complexes is determined by the phosphorylation state of PLK4 rather than STIL, then this model becomes a Type I-like system in which the dynamics which lead to symmetry breaking are indistinguishable from the Takeo et al. model.

An important benefit of the approach we outline here is that it can be mathematically proved that *all* two-component reaction-diffusion systems that break symmetry must satisfy either the Type I or Type II criteria, and that there are well-defined mathematical constraints on the parameter values required to support symmetry breaking in these systems. Nevertheless, we suspect that it will be challenging to precisely identify the molecular species that comprise A and I, and to precisely define the chemical relationship between them. This is because the interactions of PLK4 with itself (Park et al., 2014; Shimanovskaya et al., 2014; Slevin et al., 2012; Cottee et al., 2017; Leung et al., 2002; Arquint et al., 2015), with its centriole receptors (CEP152/Asl and CEP192/Spd-2) (Hatch et al., 2010; Dzhindzhev et al., 2010; Cizmecioglu et al., 2010; Sonnen et al., 2013; Kim et al., 2013; Park et al., 2014; Boese et al., 2018) and with other crucial centriole duplication proteins (such as STIL/Ana2) (Moyer et al., 2015;

Dzhindzhev et al., 2017; Ohta et al., 2018; McLamarrah et al., 2018; Moyer and Holland, 2019; McLamarrah et al., 2020) are complicated. PLK4 therefore probably binds to the centriole surface through a complex web of interactions involving several species. It is for this reason that we have not attempted here to use our modelling to make extensive predictions about the molecular identity of A and I or their precise reaction regimes.

Nevertheless, by probing these interactions in a general setting (i.e. studying the outcomes of the cases in which A and I reinforce or inhibit the various interactions in these systems) it may be possible to establish a multitude of properties that the A and I species must satisfy without explicitly knowing their composition, which in turn may help in identifying them. Indeed, by examining the outputs of Model 1 and 2, it can be seen that they make several different predictions about the behaviour of A and I under the conditions examined (compare Figures 2 and 4). For example, although A accumulates in a single peak in both models, I accumulates in the peak in Model 1 but is depleted from the peak in Model 2. This is a defining difference between Type I and Type II systems, as A generates I in the former, but suppresses it in the latter. Moreover, we can also see that in any model where phosphorylated species of PLK4 act as fast-diffusing inhibitors (e.g. Model 1) it will always be the non-phosphorylated (and so presumably kinase inactive) form of PLK4 that will accumulate to the highest levels within the single PLK4 peak. This may seem biologically implausible as PLK4 kinase activity is thought to be required to phosphorylate STIL to drive centriole assembly. However, this raises the interesting possibility that PLK4 kinase activity may be required for symmetry breaking, but not for centriole assembly. There is some evidence to support this idea (Zitouni et al., 2016; Gartenmann et al., 2020). Thus, our modelling approach allows clear predictions to be made about the behaviour of A and I in different reaction regimes. These predictions should

ultimately be testable as we generate better tools to allow us to follow the behaviour of phosphorylated and non-phosphorylated forms of the core centriole duplication proteins (Yamamoto and Kitagawa, 2019).

Finally, a potentially crucial benefit of our modelling approach is that it does not rely on PLK4 being recruited to centrioles by a number of discrete compartments, as was the case in previous models. While there is some data supporting the idea that centriolar CEP152/Asl, a major recruiter of PLK4 to the centriole (Hatch et al., 2010; Dzhindzhev et al., 2010; Cizmecioglu et al., 2010) may be organised in discrete compartments, the precise number and organisation of these compartments is unclear (Takao et al., 2019; Tian et al., 2021; Wainman, 2021; Gao et al., 2021; Tian et al., 2022; Wilmerding et al., 2023). Moreover, it has also been proposed that CEP152 may be able to self-assemble around the centriole as a continuous ring (Kim et al., 2019; Lee et al., 2020). Importantly, the reaction-diffusion models we have examined here will still break symmetry on a centriole surface comprising essentially any number of discrete compartments (Figure 5), but such compartmentalisation is not an essential requirement of our approach.

References

Arquint, C., A.-M. Gabryjonczyk, S. Imseng, R. Böhm, E. Sauer, S. Hiller, E.A. Nigg, and T. Maier. 2015. STIL binding to Polo-box 3 of PLK4 regulates centriole duplication. *Elife*. 4:1948. doi:10.7554/eLife.07888.

Arquint, C., and E.A. Nigg. 2016. The PLK4–STIL–SAS-6 module at the core of centriole duplication. *Biochemical Society Transactions*. 44:1253–1263. doi:10.1042/BST20160116.

Banterle, N., and P. Gönczy. 2017. Centriole Biogenesis: From Identifying the Characters to Understanding the Plot. *Annu Rev Cell Dev Biol*. 33:23–49. doi:10.1146/annurev-cellbio-100616-060454.

Bard, J.B. 1981. A model for generating aspects of zebra and other mammalian coat patterns. *J Theor Biol*. 93:363–385. doi:10.1016/0022-5193(81)90109-0.

Basto, R., K. Brunk, T. Vinadogrova, N. Peel, A. Franz, A. Khodjakov, and J.W. Raff. 2008. Centrosome amplification can initiate tumorigenesis in flies. *Cell*. 133:1032–1042. doi:10.1016/j.cell.2008.05.039.

Bettencourt-Dias, M., F. Hildebrandt, D. Pellman, G. Woods, and S.A. Godinho. 2011. Centrosomes and cilia in human disease. *Trends in Genetics*. 27:307–315. doi:10.1016/j.tig.2011.05.004.

Bettencourt-Dias, M., A. Rodrigues-Martins, L. Carpenter, M. Riparbelli, L. Lehmann, M.K. Gatt, N. Carmo, F. Balloux, G. Callaini, and D.M. Glover. 2005. SAK/PLK4 is required for centriole duplication and flagella development. *Current Biology*. 15:2199–2207. doi:10.1016/j.cub.2005.11.042.

Boese, C.J., J. Nye, D.W. Buster, T.A. McLamarrah, A.E. Byrnes, K.C. Slep, N.M. Rusan, and G.C. Rogers. 2018. Asterless is a Polo-like kinase 4 substrate that both activates and inhibits kinase activity depending on its phosphorylation state. *Mol Biol Cell*. 29:2874–2886. doi:10.1091/mbc.E18-07-0445.

Bornens, M. 2021. Centrosome organization and functions. *Curr Opin Struct Biol*. 66:199–206. doi:10.1016/j.sbi.2020.11.002.

Breslow, D.K., and A.J. Holland. 2019. Mechanism and Regulation of Centriole and Cilium Biogenesis. *Annu. Rev. Biochem.* 88:annurev-biochem-013118-111153. doi:10.1146/annurev-biochem-013118-111153.

Cizmecioglu, O., M. Arnold, R. Bahtz, F. Settele, L. Ehret, U. Haselmann-Weiß, C. Antony, and I. Hoffmann. 2010. Cep152 acts as a scaffold for recruitment of Plk4 and CPAP to the centrosome. *J Cell Biol*. 191:731–739. doi:10.1083/jcb.201007107.

Cottee, M.A., S. Johnson, J.W. Raff, and S.M. Lea. 2017. A key centriole assembly interaction interface between human PLK4 and STIL appears to not be conserved in flies. *Biology Open*. 6:381–389. doi:10.1242/bio.024661.

Cunha-Ferreira, I., A. Rodrigues-Martins, I. Bento, M. Riparbelli, W. Zhang, E. Laue, G. Callaini, D.M. Glover, and M. Bettencourt-Dias. 2009. The SCF/Slimb ubiquitin ligase limits centrosome amplification through degradation of SAK/PLK4. *Curr. Biol.* 19:43–49. doi:10.1016/j.cub.2008.11.037.

Dzhindzhev, N.S., G. Tzolovsky, Z. Lipinszki, M. Abdelaziz, J. Debski, M. Dadlez, and D.M. Glover. 2017. Two-step phosphorylation of Ana2 by Plk4 is required for the sequential loading of Ana2 and Sas6 to initiate procentriole formation. *Open Biol*. 7:170247–11. doi:10.1098/rsob.170247.

Dzhindzhev, N.S., Q.D. Yu, K. Weiskopf, G. Tzolovsky, I. Cunha-Ferreira, M. Riparbelli, A. Rodrigues-Martins, M. Bettencourt-Dias, G. Callaini, and D.M. Glover. 2010. Asterless is a scaffold for the onset of centriole assembly. *Nature*. 467:714–718. doi:10.1038/nature09445.

Fırat-Karalar, E.N., and T. Stearns. 2014. The centriole duplication cycle. *Curr. Biol*. 369:20130460–20130460. doi:10.1098/rstb.2013.0460.

Gao, M., R. Thielhorn, J. Rentsch, A. Honigmann, and H. Ewers. 2021. Chapter 2 - Expansion STED microscopy (ExSTED). *In* Methods in Cell Biology. P. Guichard and V. Hamel, editors. Academic Press. 15–31.

Gartenmann, L., C.C. Vicente, A. Wainman, Z.A. Novak, B. Sieber, J.H. Richens, and J.W. Raff. 2020. Drosophila Sas-6, Ana2 and Sas-4 self-organise into macromolecular structures that can be used to probe centriole and centrosome assembly. *J Cell Sci*. 133:jcs244574. doi:10.1242/jcs.244574.

Gierer, A., and H. Meinhardt. 1972. A theory of biological pattern formation. *Kybernetik*. 12:30–39. doi:10.1007/BF00289234.

Gönczy, P., and G.N. Hatzopoulos. 2019. Centriole assembly at a glance. *Journal of cell science*. 132:jcs228833. doi:10.1242/jcs.228833.

Guderian, G.G., J.J. Westendorf, A.A. Uldschmid, and E.A.E. Nigg. 2010. Plk4 trans-autophosphorylation regulates centriole number by controlling betaTrCP-mediated degradation. *J Cell Sci*. 123:2163–2169. doi:10.1242/jcs.068502.

Habedanck, R., Y.-D. Stierhof, C.J. Wilkinson, and E.A. Nigg. 2005. The Polo kinase Plk4 functions in centriole duplication. *Nat Cell Biol*. 7:1140–1146. doi:10.1038/ncb1320.

Hatch, E.M., A. Kulukian, A.J. Holland, D.W. Cleveland, and T. Stearns. 2010. Cep152 interacts with Plk4 and is required for centriole duplication. *J Cell Biol*. 191:721–729. doi:10.1083/jcb.201006049.

Holland, A.J., W. Lan, S. Niessen, H. Hoover, and D.W. Cleveland. 2010. Polo-like kinase 4 kinase activity limits centrosome overduplication by autoregulating its own stability. *J Cell Biol*. 188:191–198. doi:10.1083/jcb.200911102.

Kim, T.-S., J.-E. Park, A. Shukla, S. Choi, R.N. Murugan, J.H. Lee, M. Ahn, K. Rhee, J.K. Bang, B.Y. Kim, J. Loncarek, R.L. Erikson, and K.S. Lee. 2013. Hierarchical recruitment of Plk4 and regulation of centriole biogenesis by two centrosomal scaffolds, Cep192 and Cep152. *Proc Natl Acad Sci USA*. 110:E4849-57. doi:10.1073/pnas.1319656110.

Kim, T.-S., L. Zhang, J. Il Ahn, L. Meng, Y. Chen, E. Lee, J.K. Bang, J.M. Lim, R. Ghirlando, L. Fan, Y.-X. Wang, B.Y. Kim, J.-E. Park, and K.S. Lee. 2019. Molecular architecture of a cylindrical self-assembly at human centrosomes. *Nat Commun*. 10:1151. doi:10.1038/s41467-019-08838-2.

Klebba, J.E., D.W. Buster, T.A. McLamarrah, N.M. Rusan, and G.C. Rogers. 2015. Autoinhibition and relief mechanism for Polo-like kinase 4. *Proceedings of the National Academy of Sciences*. 112:E657–E666. doi:10.1073/pnas.1417967112.

Kleylein-Sohn, J., J. Westendorf, M. Le Clech, R. Habedanck, Y.-D. Stierhof, and E.A. Nigg. 2007. Plk4-Induced Centriole Biogenesis in Human Cells. *Dev Cell*. 13:13–13. doi:10.1016/j.devcel.2007.07.002.

Leda, M., A.J. Holland, and A.B. Goryachev. 2018. Autoamplification and Competition Drive Symmetry Breaking: Initiation of Centriole Duplication by the PLK4-STIL Network. *iScience*. 8:222–235. doi:10.1016/j.isci.2018.10.003.

Lee, K.S., J.-E. Park, J. Il Ahn, Z. Wei, and L. Zhang. 2020. A self-assembled cylindrical platform for Plk4-induced centriole biogenesis. *Open Biol*. 10:200102. doi:10.1098/rsob.200102.

LeGuennec, M., N. Klena, G. Aeschlimann, V. Hamel, and P. Guichard. 2021. Overview of the centriole architecture. *Current Opinion in Structural Biology*. 66:58–65. doi:10.1016/j.sbi.2020.09.015.

Leung, G.C., J.W. Hudson, A. Kozarova, A. Davidson, J.W. Dennis, and F. Sicheri. 2002. The Sak polo-box comprises a structural domain sufficient for mitotic subcellular localization. *Nat. Struct. Biol.* 9:719–724. doi:10.1038/nsb848.

Levin, S.A., and L.A. Segel. 1985. Pattern Generation in Space and Aspect. *SIAM Rev.* 27:45–67. doi:10.1137/1027002.

Loncarek, J., and M. Bettencourt-Dias. 2018. Building the right centriole for each cell type. *J Cell Biol*. 217:823–835. doi:10.1083/jcb.201704093.

Lopes, C.A.M., S.C. Jana, I. Cunha-Ferreira, S. Zitouni, I. Bento, P. Duarte, S. Gilberto, F. Freixo, A. Guerrero, M. Francia, M. Lince-Faria, J. Carneiro, and M. Bettencourt-Dias. 2015. PLK4 trans-Autoactivation Controls Centriole Biogenesis in Space. *Dev Cell*. 35:222–235. doi:10.1016/j.devcel.2015.09.020.

McLamarrah, T.A., D.W. Buster, B.J. Galletta, C.J. Boese, J.M. Ryniawec, N.A. Hollingsworth, A.E. Byrnes, C.W. Brownlee, K.C. Slep, N.M. Rusan, and G.C. Rogers. 2018. An ordered pattern of Ana2 phosphorylation by Plk4 is required for centriole assembly. *J Cell Biol*. 217:1217–1231. doi:10.1083/jcb.201605106.

McLamarrah, T.A., S.K. Speed, J.M. Ryniawec, D.W. Buster, C.J. Fagerstrom, B.J. Galletta, N.M. Rusan, and G.C. Rogers. 2020. A molecular mechanism for the procentriole recruitment of Ana2. *J Cell Biol*. 219:1156. doi:10.1083/jcb.201905172.

Mimura, M., and J.D. Murray. 1978. On a diffusive prey-predator model which exhibits patchiness. *Journal of Theoretical Biology*. 75:249–262. doi:10.1016/0022-5193(78)90332-6.

Montenegro Gouveia, S., S. Zitouni, D. Kong, P. Duarte, B. Ferreira Gomes, A.L. Sousa, E.M. Tranfield, A. Hyman, J. Loncarek, and M. Bettencourt-Dias. 2018. PLK4 is a microtubule-associated protein that self-assembles promoting de novo MTOC formation. *J Cell Sci*. 132:jcs219501. doi:10.1242/jcs.219501.

Moyer, T.C., K.M. Clutario, B.G. Lambrus, V. Daggubati, and A.J. Holland. 2015. Binding of STIL to Plk4 activates kinase activity to promote centriole assembly. *J Cell Biol*. 209:863–878. doi:10.1083/jcb.201502088.

Moyer, T.C., and A.J. Holland. 2019. PLK4 promotes centriole duplication by phosphorylating STIL to link the procentriole cartwheel to the microtubule wall. *eLife*. 8:570. doi:10.7554/eLife.46054.

Nigg, E.A., and A.J. Holland. 2018. Once and only once: mechanisms of centriole duplication and their deregulation in disease. *Nat Rev Mol Cell Biol*. 19:297–312. doi:10.1038/nrm.2017.127.

Nigg, E.A., and J.W. Raff. 2009. Centrioles, centrosomes, and cilia in health and disease. *Cell*. 139:663–678. doi:10.1016/j.cell.2009.10.036.

Ohta, M., K. Watanabe, T. Ashikawa, Y. Nozaki, S. Yoshiba, A. Kimura, and D. Kitagawa. 2018. Bimodal Binding of STIL to Plk4 Controls Proper Centriole Copy Number. *Cell Rep*. 23:3160-3169.e4. doi:10.1016/j.celrep.2018.05.030.

Park, J.-E., L. Zhang, J.K. Bang, T. Andresson, F. DiMaio, and K.S. Lee. 2019. Phase separation of Polo-like kinase 4 by autoactivation and clustering drives centriole biogenesis. *Nat Commun*. 10:4959–19. doi:10.1038/s41467-019-12619-2.

Park, S.-Y., J.-E. Park, T.-S. Kim, J.H. Kim, M.-J. Kwak, B. Ku, L. Tian, R.N. Murugan, M. Ahn, S. Komiya, H. Hojo, N.-H. Kim, B.Y. Kim, J.K. Bang, R.L. Erikson, K.W. Lee, S.J. Kim, B.-H. Oh, W. Yang, and K.S. Lee. 2014. Molecular basis for unidirectional scaffold switching of human Plk4 in centriole biogenesis. *Nat. Struct. Mol. Biol.* 21:696–703. doi:10.1038/nsmb.2846.

Peel, N., N.R. Stevens, R. Basto, and J.W. Raff. 2007. Overexpressing centriole-replication proteins in vivo induces centriole overduplication and de novo formation. *Curr Biol*. 17:834–843. doi:10.1016/j.cub.2007.04.036.

Rodrigues-Martins, A., M. Riparbelli, G. Callaini, D.M. Glover, and M. Bettencourt-Dias. 2007. Revisiting the role of the mother centriole in centriole biogenesis. *Science*. 316:1046–1050. doi:10.1126/science.1142950.

Rogers, G.C., N.M. Rusan, D.M. Roberts, M. Peifer, and S.L. Rogers. 2009. The SCF Slimb ubiquitin ligase regulates Plk4/Sak levels to block centriole reduplication. *J Cell Biol*. 184:225–239. doi:10.1083/jcb.200808049.

Ruan, S. 1998. Diffusion-Driven Instability in the Gierer-Meinhardt Model of Morphogenesis. *Natural Resource Modeling*. 11:131–141. doi:10.1111/j.1939-7445.1998.tb00304.x.

Shimanovskaya, E., V. Viscardi, J. Lesigang, M.M. Lettman, R. Qiao, D.I. Svergun, A. Round, K. Oegema, and G. Dong. 2014. Structure of the C. elegans ZYG-1 cryptic polo box suggests a conserved mechanism for centriolar docking of Plk4 kinases. *Structure*. 22:1090–1104. doi:10.1016/j.str.2014.05.009.

Skellam, J. 1973. The formulation and interpretation of mathematical models of diffusional process in population biology. *The Mathematical Theory of the Dynamic of Biological Populations*.

Slevin, L.K., J. Nye, D.C. Pinkerton, D.W. Buster, G.C. Rogers, and K.C. Slep. 2012. The structure of the plk4 cryptic polo box reveals two tandem polo boxes required for centriole duplication. *Structure*. 20:1905–1917. doi:10.1016/j.str.2012.08.025.

Sonnen, K.F., A.M. Gabryjonczyk, E. Anselm, Y.D. Stierhof, and E.A. Nigg. 2013. Human Cep192 and Cep152 cooperate in Plk4 recruitment and centriole duplication. *J Cell Sci*. 126:3223–3233. doi:10.1242/jcs.129502.

Sun, G.-Q. 2012. Pattern formation of an epidemic model with diffusion. *Nonlinear Dyn*. 69:1097–1104. doi:10.1007/s11071-012-0330-5.

Takao, D., S. Yamamoto, and D. Kitagawa. 2019. A theory of centriole duplication based on self-organized spatial pattern formation. *Journal of Cell Biology*. 218:3537–3547. doi:10.1083/jcb.201904156.

Tian, Y., C. Wei, J. He, Y. Yan, N. Pang, X. Fang, X. Liang, and J. Fu. 2021. Superresolution characterization of core centriole architecture. *Journal of Cell Biology*. 220:e202005103. doi:10.1083/jcb.202005103.

Tian, Y., Y. Yan, and J. Fu. 2022. Nine-fold symmetry of centriole: The joint efforts of its core proteins. *BioEssays*. 44:2100262. doi:10.1002/bies.202100262.

Turing, A.M. 1952. The chemical basis of morphogenesis. *Bltn Mathcal Biology*. 52:153–197. doi:10.1007/BF02459572.

Wainman, A. 2021. Chapter 11 - Expansion microscopy on Drosophila spermatocyte centrioles. *In* Methods in Cell Biology. P. Guichard and V. Hamel, editors. Academic Press. 217–245.

Wilmerding, A., P. Espana-Bonilla, N.-N. Giakoumakis, and M. Saade. 2023. Expansion microscopy of the chick embryo neural tube to overcome molecular crowding at the centrosomes-cilia. *STAR Protocols*. 4:101997. doi:10.1016/j.xpro.2022.101997.

Wong, Y.L., J.V. Anzola, R.L. Davis, M. Yoon, A. Motamedi, A. Kroll, C.P. Seo, J.E. Hsia, S.K. Kim, J.W. Mitchell, B.J. Mitchell, A. Desai, T.C. Gahman, A.K. Shiau, and K. Oegema. 2015. Reversible centriole depletion with an inhibitor of Polo-like kinase 4. *Science*. 1–9. doi:10.1126/science.aaa5111.

Yamamoto, S., and D. Kitagawa. 2019. Self-organization of Plk4 regulates symmetry breaking in centriole duplication. *Nat Commun*. 10:1810. doi:10.1038/s41467-019-09847-x.

Yamamoto, S., and D. Kitagawa. 2021. Emerging insights into symmetry breaking in centriole duplication: updated view on centriole duplication theory. *Current Opinion in Structural Biology*. 66:8–14. doi:10.1016/j.sbi.2020.08.005.

Zitouni, S., M.E. Francia, F. Leal, S.M. Gouveia, C. Nabais, P. Duarte, S. Gilberto, D. Brito, T. Moyer, S. Kandels-Lewis, M. Ohta, D. Kitagawa, A.J. Holland, E. Karsenti, T. Lorca, M. Lince-Faria, and M. Bettencourt-Dias. 2016. CDK1 Prevents Unscheduled PLK4-STIL Complex Assembly in Centriole Biogenesis. *Current Biology*. 26:1127–1137. doi:10.1016/j.cub.2016.03.055.

Figure 1

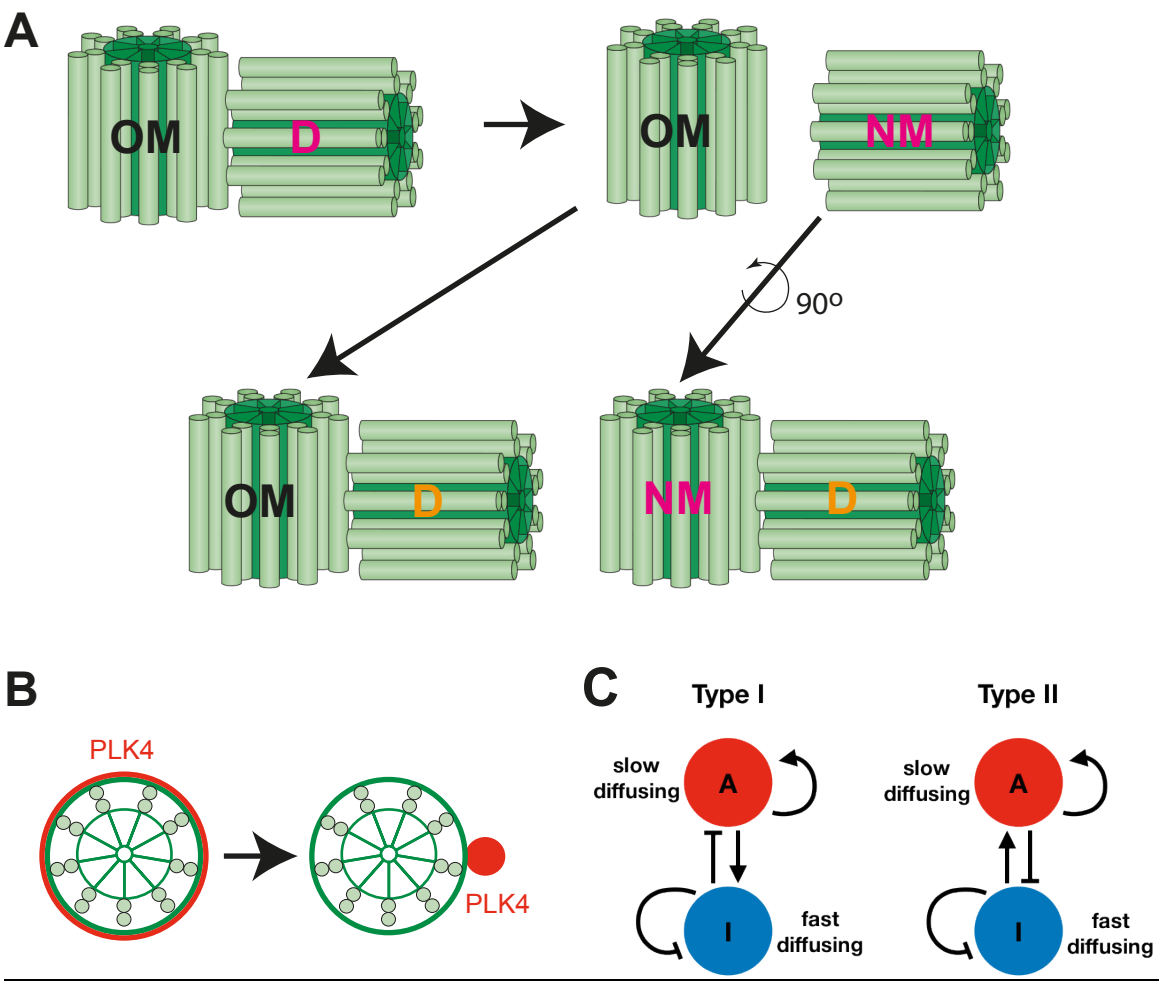

Schematic illustration of centriole duplication, PLK4 symmetry breaking, and Turing reaction-diffusion systems. **(A)** Most higher eukaryotic cells are born with a single pair of centrioles comprising an older mother (OM, labelled in *black*) and a younger daughter (D, labelled in *magenta*). This centriole pair must be duplicated prior to cell division. This occurs when the two centrioles move apart and the original daughter matures into a new mother (NM). The old mother and new mother centrioles then both give birth to a single new daughter centriole that grows perpendicularly from their sides (D, labelled in *orange*). **(B)** PLK4 (*red*) is the master regulator of centriole biogenesis, and it is initially recruited to the outer wall of the 9-fold

symmetric mother centriole barrel—viewed here looking down the barrel of the centriole (*green*). In a poorly understood process, PLK4 becomes concentrated at a single site on the side of the mother centriole that defines the site of daughter centriole assembly. **(C)** Diagrams illustrate the logic of the two chemical reaction schemes that can form Turing reaction-diffusion systems. In Type I systems, a slow diffusing Activator (A) promotes the production of more A and the production of a fast-diffusing Inhibitor (I). I inhibits the production of A and the production of I. In Type II systems, the slow-diffusing A also promotes the production of more A and the fast-diffusing I also inhibits the production of I, but A inhibits the production of I, and I promotes the production of A.

Figure 2

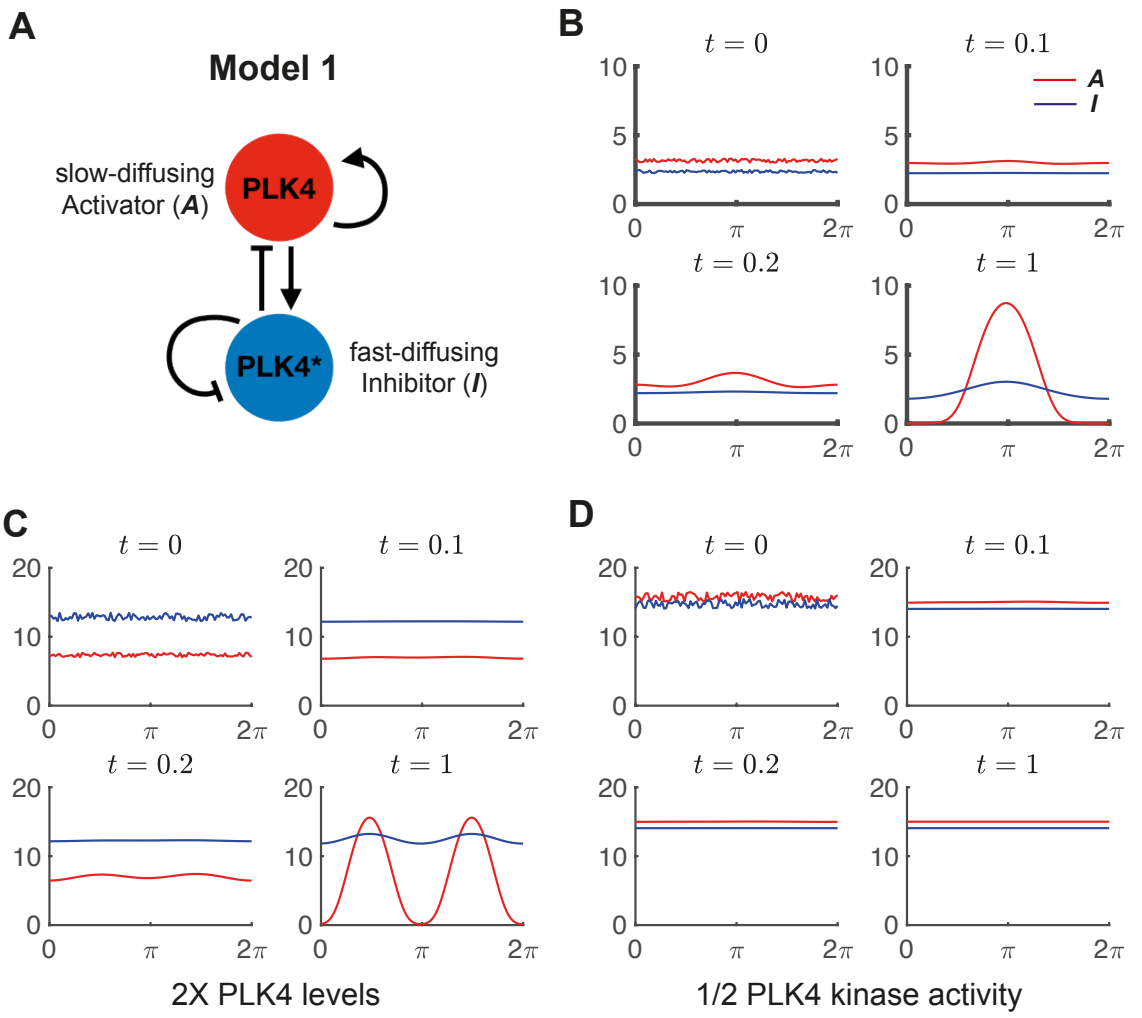

<u>An analysis of mathematical Model 1.</u> **(A)** Schematic summarises the reaction regime of Model 1, which is a Type I Turing reaction-diffusion system. The biology underlying this model was originally proposed by Takeo et al., (2018), but we have reformulated it here as a Turing reaction-diffusion system. Here, A (non-phosphorylated PLK4) promotes the production of more A through self-assembly, A promotes the production of I (PLK4*) through phosphorylation, I inhibits the production of A by converting it to I via phosphorylation, and I inhibits the accumulation of I through degradation/dissociation. **(B-D)** Graphs show how the levels of the activator PLK4 (*red* lines) and the inhibitor PLK* (*blue* lines) change over time

(arbitrary units) at the centriole surface (modelled as a continuous ring, but stretched out here as a single line between 0-2π) in computer simulations. The rate parameters for each simulation are defined in the main text and can lead to symmetry breaking to a single peak (B), or to multiple peaks when cytoplasmic PLK4 levels are doubled (C), or to no symmetry breaking at all when PLK4 kinase activity is halved (D).

Figure 3

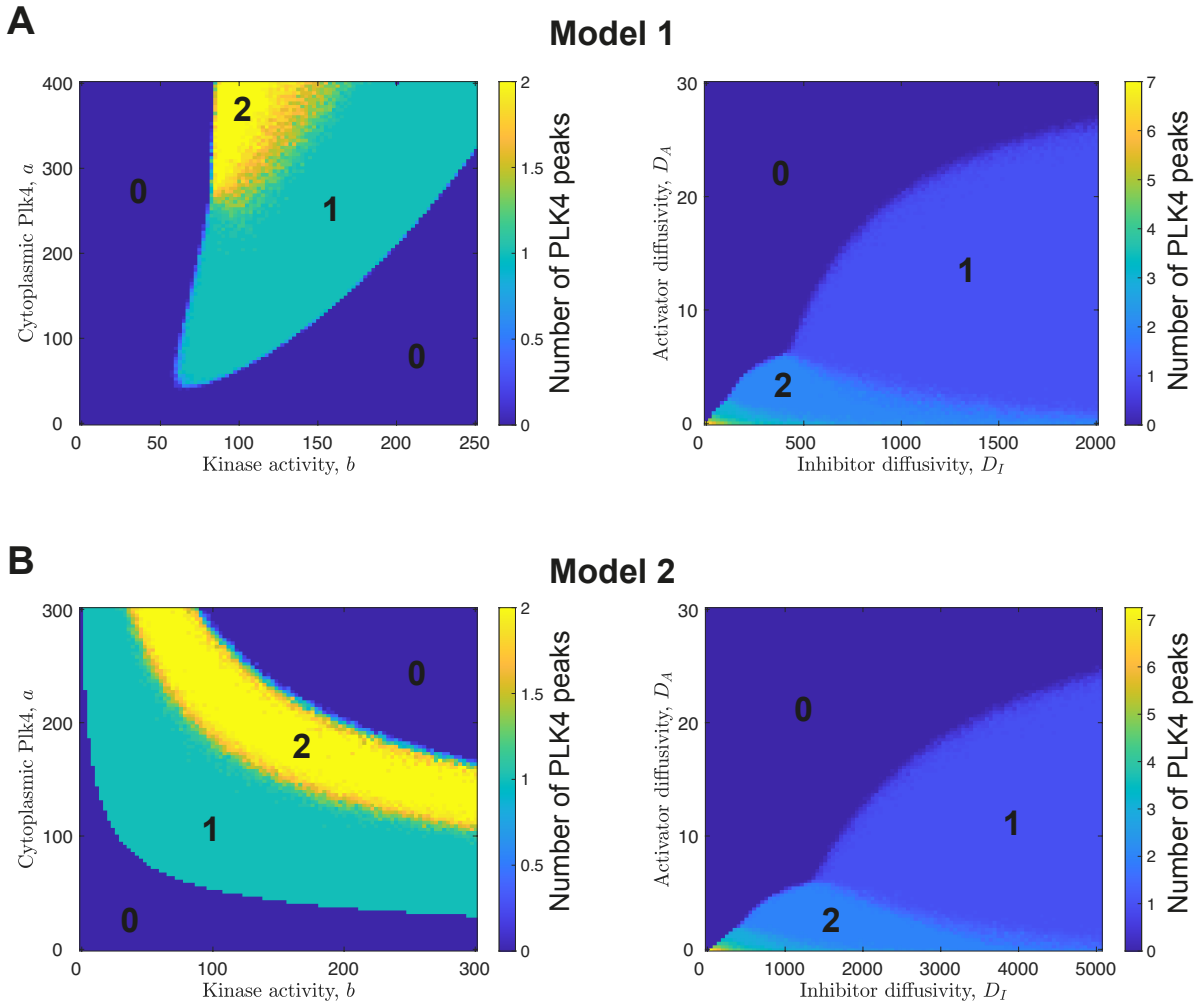

<u>Analysis of the robustness of Model 1 and Model 2 for breaking symmetry to a single peak.</u>

Phase diagrams showing how the number of PLK4 peaks generated around the centriole surface vary in Model 1 **(A)** and Model 2 **(B)** as the cytoplasmic concentration and kinase activity of PLK4 are varied (left graphs) or the diffusivity of the activator and inhibitor are varied (right graphs). Each pixel on each plot is colour-coded (scale shown to the right of each matrix) to indicate the average number of PLK4 peaks formed in 20 computer simulations. In all plots, the coloured areas mostly generating 0 (i.e. no symmetry breaking), 1 and 2 PLK4 peaks are indicated with numbers.

Figure 4

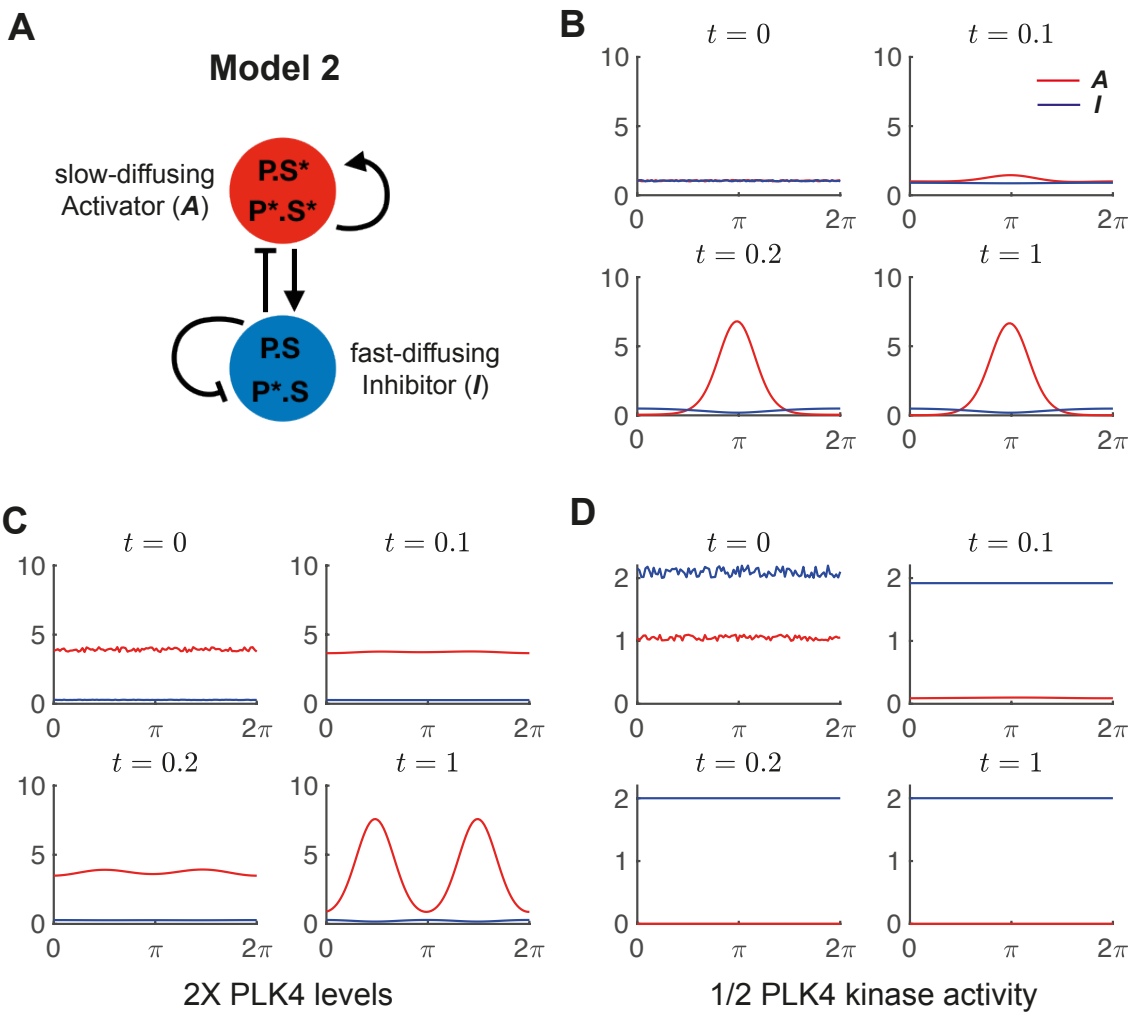

<u>An analysis of mathematical Model 2.</u> **(A)** Schematic summarises the reaction regime of Model 2, which is a Type II Turing reaction-diffusion system. The biology underlying this model was originally proposed by Leda et al., (2018), but we have reformulated it here as a Turing reaction-diffusion system in which PLK4 complexes containing phosphorylated STIL (PS^* and P^*S^*) are preferentially retained at the centriole and so act as slow diffusing activator species (that can phosphorylate more PLK4:STIL complexes to create more PS^* and P^*S^*). If STIL is dephosphorylated in these complexes (PS and P^*S), the complexes are no longer preferentially retained, so they are converted into the fast-diffusing inhibitor species that

diffuses quickly around the rest of the centriole surface, binding to the centriole surface and inhibiting the recruitment of further PLK4:STIL complexes. **(B-D)** Graphs show how the levels of the activator species (PS^* and P^*S^* – *red* lines) and the inhibitor species (PS and P^*S — *blue* lines) change over time (arbitrary units) at the centriole surface (modelled as a continuous ring, but stretched out here as a single line between 0-2π) in computer simulations. The rate parameters for each simulation are defined in the main text and can lead to symmetry breaking to a single peak (B), or to multiple peaks when cytoplasmic PLK4 levels are doubled (C), or to no symmetry breaking at all when PLK4 kinase activity is halved (D).

Figure 5

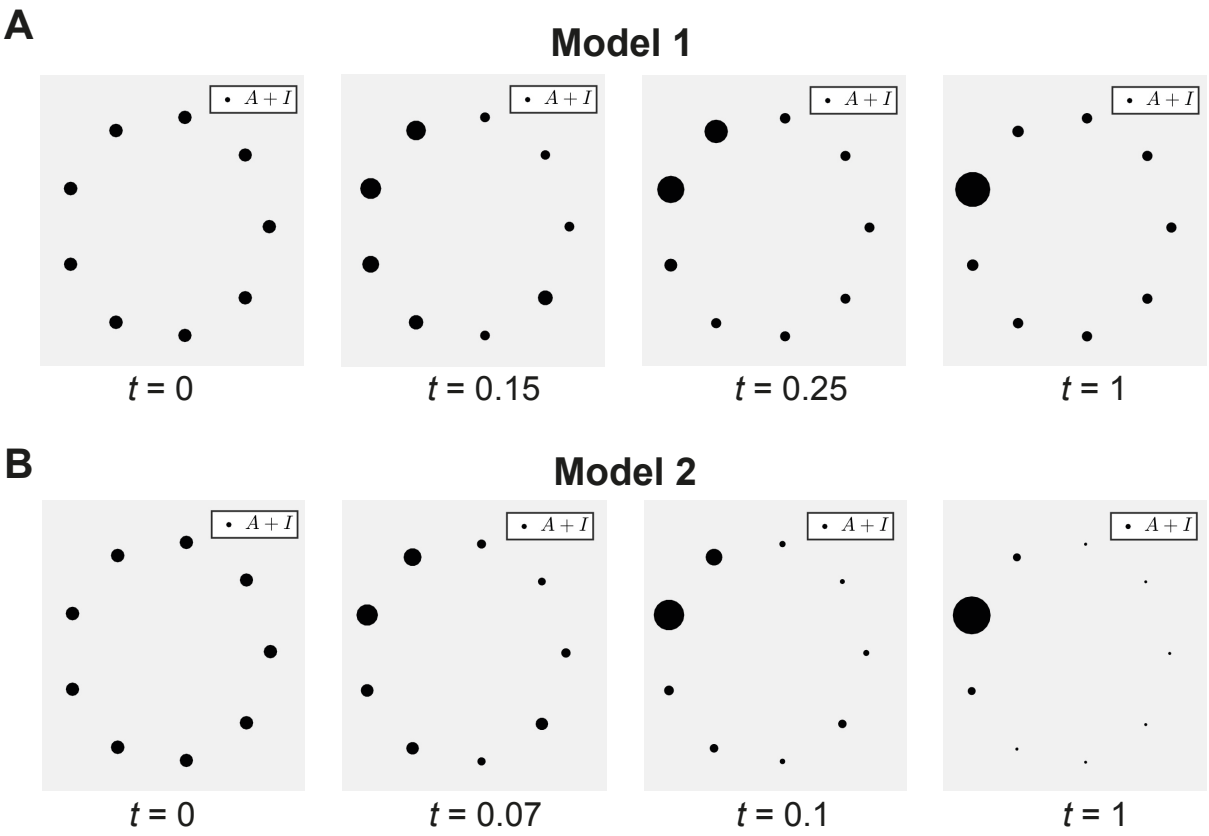

Analysis of PLK4 symmetry breaking on a 9-fold symmetric centriole surface. Diagrams show the output of computer simulations of Model 1 **(A)** and Model 2 **(B)** that have been adjusted so that the centriole is no longer one continuous surface but rather 9 independent compartments. Each compartment is depicted here as an individual dot distributed equally around the circumference of the centriole, with the size of each dot representing the amount of activator and inhibitor present in that compartment. At $t = 0$, the activator and inhibitor species are allowed to bind to and diffuse between the 9 different compartments. In both models, the system rapidly breaks symmetry, initially exhibiting a considerable variation in the amount of A and I recruited to each compartment. Both systems then rapidly settle to a dynamic steady state with a single dominant peak.